A combined approach utilizing UAV 3D imaging methods, in-situ measurements, and laboratory experiments to assess water evaporation and trace element uptake by tree species growing in a red gypsum landfill

Abdoulaye Mahamat Malabad, Fabienne Tatin-Froux, Gilles Gallinet, Jean-Michel Colin, Michel Chalot, Julien Parelle

A combined approach utilizing UAV 3D imaging methods, *in-situ* measurements, and laboratory experiments to assess water evaporation and trace element uptake by tree species growing in a red gypsum landfill

Abdoulaye Mahamat Malabad[a], Fabienne Tatin-Froux[a], Gilles Gallinet[b], Jean-Michel Colin[c], Michel Chalot[a,d], Julien Parelle[a]*

[a] Chrono-environnement UMR6249, CNRS, Université Bourgogne Franche-Comté, F-25000, Besançon, France

[b] Hekladonia SAS, 242 Boulevard Voltaire, 75011 Paris, France

[c] TRONOX, 95 Rue du Général de Gaulle, 68800 Thann, France

[d] Université de Lorraine, Faculté des Sciences et Technologies, 54000 Nancy, France

*Corresponding author: Laboratoire Chrono-environnement, UMR 6249, CNRS, Université Bourgogne Franche-Comté, 16 Route de Gray, 25030 Besançon cedex, France.

E-mail address: julien.parelle@univ-fcomte.fr (J. Parelle).

Abstract

The extractive industry is increasingly faced with problems of managing contaminated sites. The red gypsum landfill at the Ochsenfeld site is representative of the typology byproduct storage of the Ti-extraction activity. The management of the elemental content and the water body are the issues at this site. The aim of this study was to evaluate the canopy conductance (g_{cmax}) of various tree species and the content of elements in the leaves, utilizing the opportunity of a demonstration plantation setup in 2014 with sixteen tree species, combined with a growth chamber experiment. We combined the gas exchange measurements with the data from two multispectral cameras with RGB and NIR bands embarked on an unmanned aerial vehicle (UAV). In the field, *Ostrya carpinifolia, Maclura pomifera,* and *Rhus copallina* had the highest g_{cmax} of all planted tree species, and the high transpiration rate in *O. carpinifolia* was confirmed in a pot-based controlled experiment. Except *R. copallina*, the species with a high Mn content (*O. carpinifolia*, *Betula pendula*, and *Salix aquatica grandis*) had high stomatal conductance. *O. carpinifolia* could therefore be a species to exploit in the management of landfill leachates, especially in the context of climate change since this species is well adapted to dry environments.

Keywords: UAV Remote Sensing; LAI; Canopy conductance; Transpiration; *Ostrya carpinifolia*

1. Introduction

According to the Joint Research Centre (JRC), since the 1970s, the extraction of metals has increased by more than 75% worldwide (Joint Research Centre, 2017). This significant increase in extractive activities has had a strong impact on the environment. In European Union countries, there are overall between 150,000 and 500,000 mine landfills, the majority of which are no longer active (Vaverková, 2019), which raises the question of the management of these landfills. Red gypsum landfills represent an environmental and ecological model of the typology of byproduct storage of Ti-extraction activity (high content of some trace elements (TEs): notably Fe and Mn and low biodiversity) (Edraki et al., 2014; Huang et al., 2012; Zapata-Carbonell et al., 2020). Extraction of Ti from ilmenite using the sulfuric process leads to the production of red gypsum during the neutralization of the company's wastewater with limestone. This red gypsum, accumulated over decades, allows the formation of a technosol, on which the development of vegetation is lessened due to the presence of various mineral oxides and TEs (Ciadamidaro et al., 2019; Zapata-Carbonell et al., 2019). The lack of vegetation potentially leads to mineral (including TEs) leaching and dust enriched in TEs. Moreover, this red gypsum is stored on a waterproof structure that requires appropriate management of the incoming and outgoing water masses. The revegetation of landfills is therefore an important issue to better manage water flows via evapotranspiration and to limit the spread of dust. Phytomanagement, which has recently become an alternative for site and soil management, comprises a set of sustainable techniques using tree species *in situ,* for example, to restore some ecosystem services, to control erosion, and more relevantly here to regulate water flow (Cundy et al., 2016). Trees indeed contribute to water balance through transpiration. Using a lysimeter-based approach, *Populus* sp. was found to enhance evapotranspiration and to reduce bore leaching by accumulation in aerial biomass (Robinson et al., 2007). Important mass flow may enhance plant nutrient acquisition by promoting the movement of nutrients from the soil to the root and aerial parts of the plant (Huang et al., 2017). Mn moves freely in the xylem sap and is transported to leaves via transpiration stream with little redistribution (Ducic and Polle, 2005). Barber (1995) described and modelled nutrient uptake by crop tree species and concluded that the water flux is a key parameter. Element uptake modelling was used to describe K, P, Zn and Mn uptake by different tree species and to further demonstrate the role of water flux (Adhikari and Rattan, 2000; Brouder, 1994; Chen, 1990; Sadana and Claassen, 2000). Previous studies have reported negative relationships between

63 foliar TE content and transpiration rate in tree species (Kitao et al., 1997; Milan, 2012; Pajevic et al.,
64 2009; Arsenov et al., 2020). In plants, metals exert their toxic action, mostly by damaging chloroplast
65 and disturbing photosynthesis and the inhibition of photosynthesis is the consequence of interference of
66 metal ions with photosynthetic enzymes and chloroplast membranes, thus inducing a biochemical
67 limitation of stomatal conductance, as reviewed in Aggarwal et al., (2011). Many studies have shown
68 that an excess supply of TEs leads to significant changes in the water relations of tree species (Pandey
69 and Sharma, 2003; Vernay et al., 2007). It has also been observed in experiments conducted under
70 greenhouse conditions with *Populus* hybrids that the transpiration rate decreased with an increase in
71 mixed TE (Cd, Cr, Cu, and Zn) content (Chandra and Kang, 2016). The transpiration rate and stomatal
72 conductance in *Phaseolus vulgaris* were reduced by a high Zn content (Van Assche et al., 1980) or by
73 $ZnSO_4$ at 600 mg/kg in peat moss soil (Kasim, 2007). Mn, which is one of the major components of the
74 red gypsum sediment at the Ochsenfeld site (Zapata-Carbonell et al., 2019), accumulates predominantly
75 in the plant shoot (Page et al., 2006). High Mn content leads to excess TE deposition in photosynthetic
76 cells and might potentially impair cellular metabolism (Fernando et al., 2013), which may lead to metal
77 toxicity in cells. High Mn content can decrease the net photosynthetic rate, stomatal conductance,
78 internal carbon dioxide concentration and transpiration in several genotypes of cotton (Tavanti et al.,
79 2019). The transpiration of plants depends not only on tree species physiology, *i.e.,* the ability to regulate
80 the stomatal aperture but also the leaf area. The transpiration capacity is estimated by the transpiring
81 surface of plants and thus by the leaf area index (LAI). This index is the ratio between the sum of the
82 foliar area and the unit of ground area (Watson, 1947). LAI is traditionally obtained by harvesting all
83 leaves of a plot and by measuring the surface of each leaf. Modern alternative methods have been
84 developed. Flatbed scanners have made this process more efficient, but it is still laborious, time
85 consuming and destructive. It is possible to use instruments based on atmospheric sensors (LI-COR
86 LAI-2000 Plant Canopy Analyser and CI-100 Plant Canopy Analyser) or a linear array of
87 photosynthetically active radiation sensors (AccuPAR Ceptometer) to estimate the LAI (Breda, 2003;
88 Peper and McPherson, 1998; Wilhelm et al., 2000). These indirect non-destructive techniques comprise
89 the application of a logarithmic regression and allometric equation, which is faster to set up for
90 homogeneous covers but has not yet been applied for multispecific row plantations (Nowak, 1996). As
91 the alternative method, the Light Detection and Ranging (LiDAR) can be used as an active sensor which

92 is based on the emission of a highly collimated laser pulse and analysing the reflected signal (Lin, 2015)
93 to estimate LAI using volumetric methods such as surface differencing (Loudermilk et al., 2009) where
94 the digital terrain model (DTM) is subtracted to the digital surface model (DSM). In a recent review
95 (Wang and Fang, 2020), where LiDAR technology, LAI retrieval and validation methods are reviewed,
96 it is concluded that terrestrial laser scanning (TLS), airborne laser scanning (ALS) or spaceborne laser
97 scanning (SLS) data can used for the estimation of the vegetation LAI. While the use of LiDAR for the
98 estimation of LAI have shown promising results especially in forest application (Alonzo et al., 2015;
99 Lefsky et al., 1999), other approaches have been developed. Among these new technologies, the use of
100 unmanned aerial vehicles (UAVs) to record low-altitude images is becoming increasingly widespread
101 (Zhang and Kovacs, 2012) and is the only automated alternative for heterogeneous cover. LAI
102 estimation from UAV-based remote sensing multispectral imagery (Hunt et al., 2008) is increasingly
103 reported, for instance in agriculture (Yao et al., 2017), in mangrove (Tian et al., 2017) and forest (Lin et
104 al., 2021) ecosystems. Although UAV have been used in landfill monitoring (Rauhala et al., 2017;
105 Shahmoradi et al., 2020), to our knowledge, no studies have been conducted on the use of UAV to
106 estimate LAI at landfills under phytomanagement. Most authors have used vegetation indices based on
107 photogrammetry analysis, such as the normalized difference vegetation index (NDVI), which is used to
108 monitor the degree of vegetation greenness (Tucker, 1979; Zarco-Tejada et al., 2012). NDVI data have
109 proven to be a robust approach for estimating biotic stress (chlorophyll deficiency) and abiotic stress
110 (water drought). NDVI is a rate of operation of reflectance per specific bands (NIR-R/NIR+R) for
111 multispectral signature where NIR and R are respectively the near-infrared and red bands. It is also a
112 measure of reflectance and an estimation of vegetation growth and biomass (Gandhi et al., 2015);
113 however, this index is not quantitative and has to be calibrated using field data.
114 The present study focuses on the Ochsenfeld red gypsum landfill, located in northeastern France, with
115 an area of 80 ha. The main management issues at the Ochsenfeld site are (i) to revegetate the site to
116 stabilize the soil, thus limiting the dispersion of dust and TEs, or for producing a valuable Mn-enriched
117 biomass and (ii) to increase the evapotranspiration potential of the site, thus reducing the volume of
118 water stored in the landfill that remains to be treated. On part of the site, we set up a phytomanagement
119 trial in 2014 with different tree species to select the tree species best suited to the site conditions
120 (Ciadamidaro et al., 2019). Considering these particular objectives and conditions, our hypothesis was

121 that the selection of tree species for TE uptake capacity would not be antagonist to the selection of
122 species with a high transpiration rate. The opportunity of the 5-year-old demonstration plantation was
123 used to estimate leaf area with a surface integration method using UAV-based remote sensing, to screen
124 transpiration capacity and to determine TE content in leaves. The leaf surface and surface area of the
125 trees were originally developed using a surface integration method to quantitatively estimate the LAI.
126 In the present study, we further used low-altitude photos obtained with UAVs that allow three-
127 dimensional integration to obtain developed surfaces. The transpiration rate of some selected tree species
128 growing on anthroposol from Ochsenfeld site and its relationship with the Mn content were further
129 explored under controlled conditions with a more accurate method (by utilizing the weight loss method)
130 to potentially confirm the field results. The objectives of these experiments were (i) to test the method
131 of LAI estimation by using UAV 3D-imaging-based remote sensing on landfill, (ii) to combine LAI
132 estimation by using UAV 3D-imaging and gas exchange measurements for estimating the maximum
133 canopy cover conductance as an estimator of tree performance for their capacities of management of
134 water flow, and (iii) to test a potential concomitance between transpiration performance and leaf element
135 uptake performance in a phytomanagement context.

136 ## 2. Materials and methods

137 ### 2.1. Experimental design

138 #### 2.1.1. Field experiment

139 The pilot site of a 1-ha area was implemented in April 2014 on a storage landfill of mining byproducts
140 located in the municipality of Thann in Northeast France (Fig. 1) and was fully described by
141 Ciadamidaro et al. (2019). The soil has silty and alkaline characteristics and is enriched mainly in Mn,
142 Fe, and S (Assad et al., 2017). A 30 cm layer of backfill was added on top of the red gypsum before
143 planting. According to Ciadamidaro et al. (2019), only 16 species of the 18 planted species with a
144 significant growth performance were selected for this study (Table 1).

145 Table 1. List of the tree species used in the present study and their abbreviations

Abu	*Acer buergerianum*	Por	*Platanus orientalis*
Agi	*Acer ginnala*	Pst	*Pterocarya stenoptera*

Bpa	*Betula papyrifera*	Qac	*Quercus acutissima*
Bpe	*Betula pendula*	Rco	*Rhus copallina*
Csp	*Catalpa speciosa*	Sag	*Salix aquatica grandis*
Csi	*Cedrela sinensis*	Sal	*Salix alba*
Mpo	*Maclura pomifera*	Upu	*Ulmus pumila*
Oca	*Ostrya carpinifolia*	Zse	*Zelkova serrata*

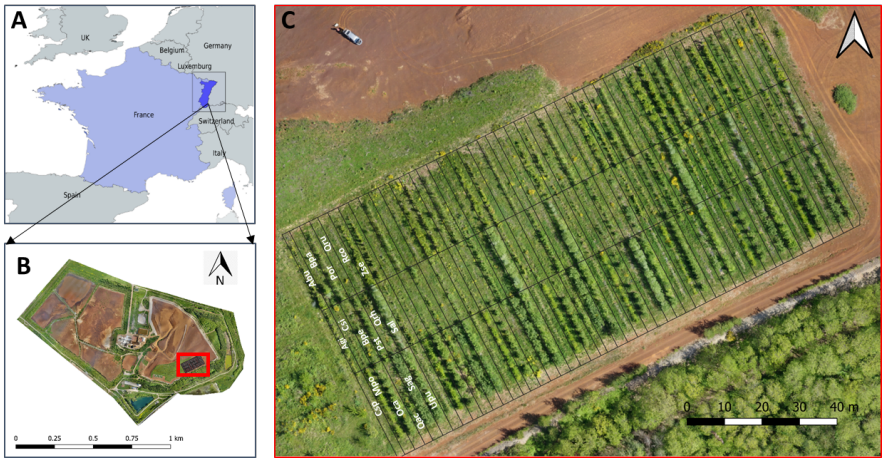

Fig. 1. The experimental Ochsenfeld site at Thann (France). (A) Geographic location of the red gypsum landfill. (B) Aerial view of the site showing the location of the experimental plot (red rectangle). (C) Partition of the experimental area: each partition corresponds to the plantation of one row of one species, and 8 rows were planted per species.

2.1.2. Growth chamber experiment

A pot experiment was performed in a controlled growth chamber on five tree species showing contrasting growth and elemental contents in the leaves (according to Ciadamidaro et al., 2019): *B. pendula*, *S. aquatica grandis*, *O. carpinifolia*, *P. stenoptera*, and *A. buergerianum* (20 plants per species). *B. pendula* seeds were collected from the Ochsenfeld site and sown on peat (Brill Typical, Germany) for 3 months. *O. carpinifolia*, *P. stenoptera* and *A. buergerianum* seedlings and *S. aquatica grandis* seedlings were provided by Soupe Nursery (Chatillon sur Chalaronne, France). They were grown directly on the anthroposol at the Ochsenfeld site in 4 L pots. The climatic conditions present for the growth chamber experiments were as follows: day illumination duration of 16 h; night time of 8 h; day/night temperature of 23 °C/21 °C; day/night humidity of 70%; and day illumination intensity of

approximately 600 µmol/m^2/s of photon photosynthetic activity. The measurements were conducted at intermediate (90 days) and final times (152 days).

2.2. Ecophysiological analysis

For the field experiment, the maximum stomatal conductance (g_{smax} expressed in mol H_2O/leaf m^2/s) was monitored between June and July 2019 on one fully sun-exposed leaf (n=9 randomly chosen by species) using a portable gas-exchange system (Licor-6400 Lincoln, Nebraska) at 400 ppm CO_2, 30 °C block temperature, photosynthetically active radiation at 1400 µmol/m^2/s and ambient air humidity (min = 50% and max = 80%). Each measurement was recorded when the stabilization of g_{smax} was observed (approximately 3 min). Minimum leaf water potentials (Ψ_{min} expressed in MPa) were measured immediately after on the same twig with a pressure chamber (Scholander et al., 1965). These measurements were collected between 10 a.m. and 4 p.m. local time to ensure light conditions supported maximum photosynthetic rates and minimum Ψ_{min}.

For the growth chamber experiment, the plant transpiration stream was measured through water loss method by weighing pots packed in a plastic bag for 4 h to limit the evaporation of the soil. To express the transpiration per unit leaf area, an estimation of the total leaf area was performed by measuring the leaf length of all leaves of each measured plant. The etalon curve leaf area – leaf length and leaf area – and leaf dry mass, realized for intermediate time and final time measurements, respectively, were measured for a subset of leaves from each species with a WinRHIZO scanner (Regent Instrument, Quebec, Canada). Details of the equations used are provided in the supplemental information Fig. S1.

2.3. Remote sensing

UAV-based remote sensing was used to calculate the height of tree species and vegetation indices (LAI and NDVI). Two high-resolution digital cameras, Sony (RX100 M3; Tokyo, Japan) for red (R: 620 to 670 nm), green (G: 490 to 570 nm), and blue (B: 450 to 490 nm) bands and Canon (S110; Tokyo, Japan, modified by LDP LLC Max, Carlstadt, USA) for near-infrared (NIR: 680 to 800 nm) bands with a resolution of 8 megapixels, were embarked on the drone TurtleQuad® designed by Gilles Gallinet. On 24 May 2019, on a clear and sunny day a flight of the UAV was conducted aloft at 30 to 35 metres from the ground between 11:30 a.m. and 12:40 a.m. local time to collect spectral radiance at ground from aerial photos. A total of 547 photos were taken to generate the first 3-D model (dense cloud and shaded

model) using Metashape-AGISOFT photogrammetric software (version 1.6.1, Agisoft LLC, Saint Petersburg, Russia). This 3-D model used 11 ground targets (GCPs) for the 3-dimensional calibration of the photogrammetric model, recorded by traditional terrestrial acquisition using a high-precision real-time kinematic - global positioning system (RTK-GPS). From this 3-D model, still using Metashape-AGISOFT, an orthomosaic projection generated two multiband orthophotographs: one with red (band1), green (band2), and blue (band3) bands, and the second with near-infrared (band1), green (band2), and blue (band3) bands. The data from these multiband orthophotographs were then processed using QGIS version 3.10.1-A Coruña (QGIS Development Team, 2018).

The source images had the following resolution: 9.89 mm/pix for RGB and 1.46 cm/pix for NIR. The two RGB and NIR orthomosaics were first calculated using Metashape, each separately with their native resolution. They were then resampled when exported by Metashape to provide images with a GSD (Ground Spatial Distance) of 10 cm/pix. Processing in QGIS was then performed with this resampled resolution of 10 cm/pix for all bands used. The sampling algorithm during orthomosaïc generation process and the resampling algorithm during export were the same *i.e.* bilinear interpolation. The geometric calibration of the optics was carried out using the Metashape software, which has built-in tools for this. The overlay between the captured images was chosen to be greater than 80% in both length and width. Furthermore, the flight lines overlapped. Therefore, each pixel of the orthomosaïc was calculated from at least nine photographs (see supplemental information Fig. S2 and S3). The mapping was deliberately done beyond the perimeter of the study area to avoid any edge effect. The maps extended at least 25 m beyond the lateral limits of the actual study area.

The tree height (TH) was calculated in QGIS by calculating the difference in altitude between the DSMs and the DTM (Eq. 1). The DSM was the 3D surface of the cover canopy of vegetation. The precision of the DSM was x = 3 cm, y = 3 cm and z = 5 cm. The DTM was a 3-D area of the soil without vegetation. The DTM was recorded by traditional terrestrial acquisition using a high precision RTK-GPS. This DTM integrated the reading of the 11 ground targets used for the 3-dimensional calibration of the photogrammetric model. The accuracy of the RTK GPS reading on the ground was x, y = 1 cm and z = 2 cm. The soil DTM and vegetation canopy DSM were in the same projection system and the same altimeter setting.

$$TH = DSM - DTM$$

(1)

To obtain the LAI, we calculated the ratio between the leaf area of canopy cover (LA) and the area projected at the ground of the canopy cover (GC) of the tree species (Eq. 2). The leaf area of the canopy cover was measured on Agisoft Metashape by manual delineation of the tree crown (Fig. 2). The area of the canopy cover projected on the ground was calculated on QGIS also by manual delineation of the tree crown.

$$LAI = \frac{LA}{GC}$$

(2)

The LAI multiplied by the mean of the g_{smax} allowed us to obtain the canopy conductance (g_{cmax} expressed in mol H_2O/ground m^2/s), which is controlled mainly by these two variables (Granier et al., 2000).

The NDVI values were calculated according to the following equation (Eq. 3) using QGIS, where NIR and R are reflectance values in the near-infrared and red wavelengths, respectively, given by Tucker (1979). The NDVI values range from 0.2 to 0.8 for vegetation and are unitless. High NDVI values indicate healthy and dense green vegetation, and low NDVI values indicate moisture-stressed and sparse vegetation (Drisya et al., 2018; Gessesse and Melesse, 2019).

$$NDVI = \frac{NIR - R}{NIR + R}$$

(3)

The experimental site was divided into eight different plots as described by Ciadamidaro et al. (2019). Each plot consisted of a replicate of the 18 different tree species planted in rows (one row by species). For the present UAV-based study, the experimental site was partitioned row-by-row, constituting eight replicates per species (Fig. 1C). The results for each species were the median and the quartiles of these eight rows.

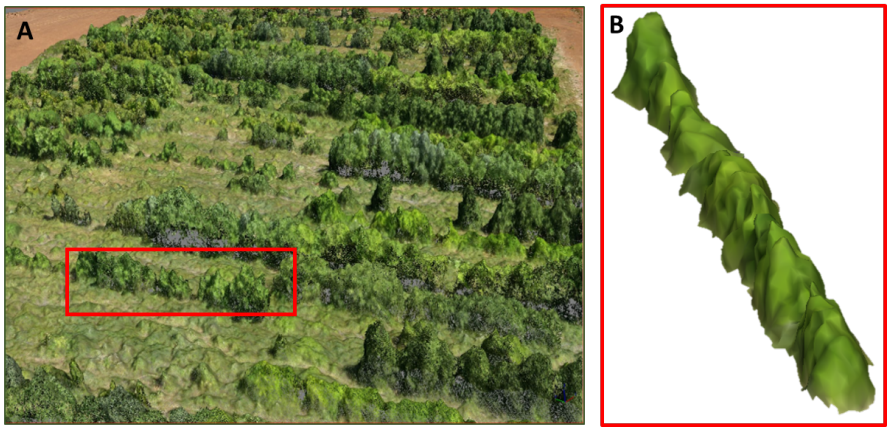

Fig. 2. Three-dimensional UAV view of the canopy cover at the experimental Ochsenfeld site. (A) General view of the demonstration site generated at-sensor reflectance orthomosaics using Metashape-AGISOFT photogrammetric software. (B) Detailed view of one plot corresponding to one tree species obtained by manual delineation of the tree crown. Each row of a tree species was cut, isolated and trimmed, which further allowed us to estimate the developed leaf area using a surface integration method.

2.4. Elemental analysis

For each tree species, the leaves used for gas exchange measurements were washed with deionized water and dried at 70 °C for 72 h. These dried leaf samples were ground using a ball mill (Retsch MM300, Eragny, France). Mineralization was realized by acid digestion with concentrated HNO_3 using a VELP DK6 heating digester (VELP Scientifica, Usmate Velate, Italy). As described by Assad et al. (2017), the total elemental content (Al, B, Ca, Cd, Cu, Fe, K, Mg, Mn, Na, P, S, Si, Sr, Ti, and Zn) in the leaves from the field samples was determined using inductively coupled plasma atomic emission spectrometry (ICP-AES, Radial ICAP 6500 Model, Thermo Fischer Scientific, Inc., Pittsburgh, USA). For the pot experiment, Mn content was determined by atomic absorption spectroscopy (AAS, Agilent Technologies, Inc., Santa Clara, USA).

2.5. Statistical Analysis

All statistical analyses were performed using R software version 4.0.4, the R Foundation for Statistical Computing (R Core Team, 2021), at a significance level when $P < 0.05$. To verify the homoscedasticity and the normality of the all dataset, we had used a Levene test (Levene, 1960) and Shapiro–Wilk test (Shapiro and Wilk, 1965) respectively. As dataset did not fit the assumption of the normal distribution,

they were analysed with non-parametrical tests. For all considered variables, the statistically significant difference between tree species within a variable was analysed using a Kruskal-Wallis test by ranks. Spearman's rank-order correlation was performed to compare the different variables assayed and to compare the rank of different tree species for each variable. A confusion matrix with a 10-fold cross-validation was performed to estimate the generalized accuracy average and to evaluate confusion between the different tree species, using caret package (version 6.0-90).

3. Results

3.1. *In-situ* measurements

3.1.1. Transpiration proxies

We observed significant differences in g_{smax} and Ψ_{min} values among the 16 tree species (Fig. 3). *O. carpinifolia, R. copallina* and *M. pomifera* exhibited significantly higher g_{smax} to water vapour than a group of 11 other species (Fig. 3A). The two species, *S. aquatica grandis* and *B. pendula*, had intermediate g_{smax} values. The Ψ_{min} ranged from -2.27 to -0.09 MPa, with Ψ_{min} values of -0.28 ± 0.13 MPa and -2.03 ± 0.08 MPa for *M. pomifera* and *A. ginnala*, respectively (Fig. 3B). The rank of the different tree species for their Ψ_{min} value was significantly similar to the rank obtained for the g_{smax} values (Spearman rank correlation with P = 0.003), suggesting that the two proxies could be used for estimating differences in the transpiration stream. As exceptions, *M. pomifera* and *R. copallina* combined a high g_{smax} with a high Ψ_{min}.

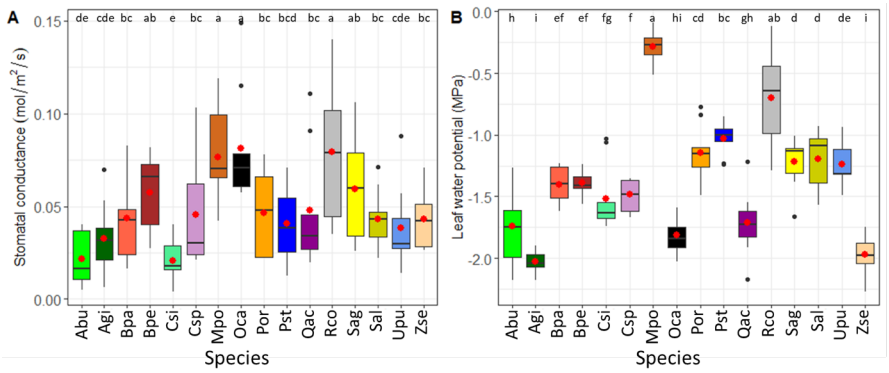

Fig. 3. Transpiration proxies (mean (red dot), median, quartiles, range, and outliers) (n=9). (A) g_{smax} (mol H_2O/leaf m^2/s) and (B) Ψ_{min} (MPa), measured on the 16 tree species growing at the experimental Ochsenfeld site. Boxes with the same letter did not differ significantly from each other using a pairwise Kruskal−Wallis test ($P < 0.05$).

The analysis of the Ci (concentration of CO_2 in the intercellular spaces of the leaf) versus g_{smax} graph underlined that for the two species, *C. sinensis* and *A. buergerianum*, the lowest conductance might be attributed to a biochemical limitation (Fig. 4). These two species were clearly limited in their CO_2 assimilation among all tested tree samples, with a negative correlation between Ci and g_{smax}. The other species, *e.g., O. carpinifolia*, *R. copallina* and *M. pomifera,* seemed to cope better with the soil conditions.

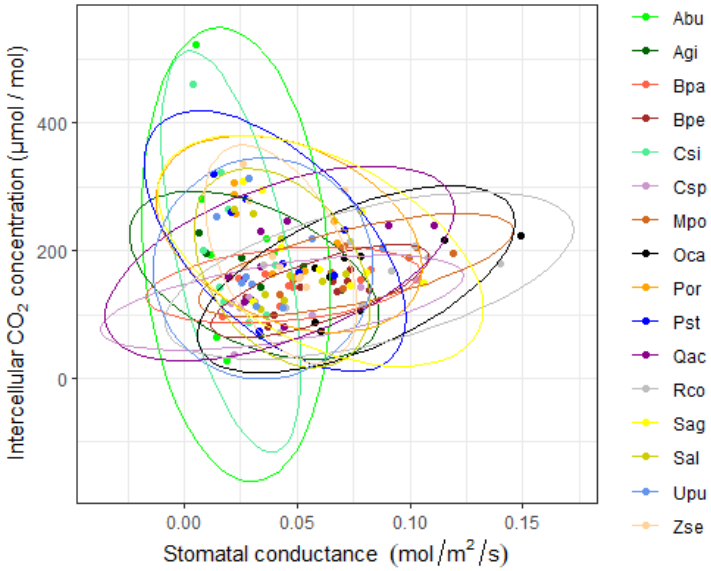

Fig. 4. Relationship between intercellular CO_2 concentration (Ci expressed in µmol CO_2/mol air) and maximal stomatal conductance to water vapour (g_{smax} expressed in mol H_2O/leaf m^2/s) for the 16 tree species growing at the experimental Ochsenfeld site. Each colour represents one of the 16 trees studied, with 9 measurements per tree, and ellipses correspond to the 0.95 confidence interval.

3.1.2. Remote sensing

UAV-based remote sensing allowed us to obtain the tree height (expressed in m) (Fig. 5A), LAI (expressed as the ratio of m^2 of leaf area to m^2 of ground area, Fig. 5B), and NDVI value (Fig. 5C) of the tree species present at the Ochsenfeld site. For these three parameters obtained using UAV-based

303 remote sensing, the rank order of the tree species was highly similar, with $P < 0.001$ (Spearman's rank-
304 order correlation). We further combined the LAI data (Fig. 5A) and g_{smax} data (Fig. 3A) to obtain the
305 maximal canopy conductance (g_{cmax} expressed as mol H_2O/ground m^2/s, Fig. 5D).
306 *U. pumila, O. carpinifolia, M. pomifera, S. aquatica grandis* and *P. orientalis* had the greatest heights
307 among the tree species planted at the Ochsenfeld site in 2014, whereas *A. ginnala*, *C. speciosa*, *Q.*
308 *acutissima*, *B. pendula* and *B. papyrifera* had the lowest heights. The other tree species had an
309 intermediate height (Fig. 5A). The LAI data followed the same trend, with *U. pumila, O. carpinifolia,*
310 *P. orientalis, S. aquatica grandis* and *M. pomifera* having the greatest LAI values, while *A. ginnala* and
311 *B. pendula* had the lowest LAI values (Fig. 5B). The NDVI values for the study area plotted in the 0.23
312 (*A. ginnala*) - 0.40 (*O. carpinifolia*) range (Fig. 5C), which reflects the difference in tree growth and
313 cover as discussed above. As an exception, the *P. stenoptera* species, despite a relatively low height,
314 had one of the highest NDVI values. With the highest LAI and g_{smax} values, *O. carpinifolia* had the
315 greatest g_{cmax} (Fig. 5D), while *A. ginnala* had values 10 times lower than those of *O. carpinifolia*. Among
316 the tree species studied, only *O. carpinifolia*, *M. pomifera*, *R. copallina*, *S. aquatica grandis*, *U. pumila*,
317 *P. orientalis* and *C. speciosa* had on average a g_{cmax} greater than 0.1 mol H_2O/ground m^2/s.

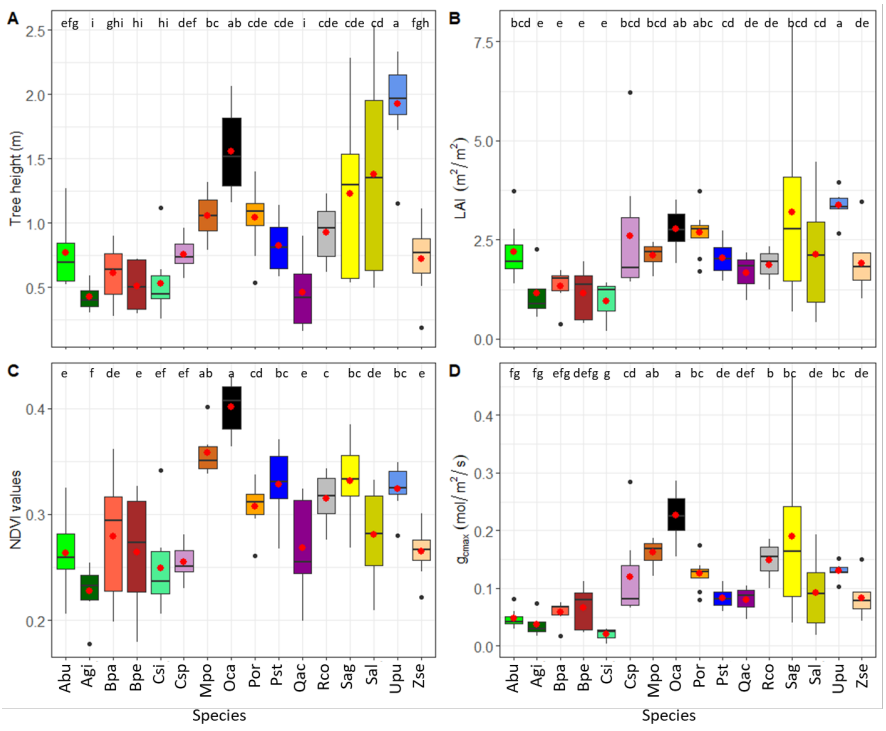

Fig. 5. UAV-based remotely sensed parameters of the 16 tree species growing at the experimental Ochsenfeld site (mean (red dot), median, quartiles, range, and outliers) (n=8). (A) Tree height (m), (B) LAI values (leaf m^2/ground m^2), (C) NDVI values and (D) g_{cmax} (mol H_2O/ground m^2/s). Boxes with the same letter did not differ significantly from each other based on a pairwise Kruskal–Wallis test ($P < 0.05$).

3.1.3. Foliar elemental content and leaf water status

The elemental content detected in leaves was significantly different among species (Fig. 6). Mn, the major element to be considered for the management of red gypsum sediment, was found in greater amounts in species belonging to the Betulaceae (*B. pendula*, *B papyrifera*, and *O. carpinifolia*) and Salicaceae (*S. alba* and *S. aquatica grandis*) families. *B. pendula* and *O. carpinifolia* had the highest Mn contents, with values 3 times greater than those of *C. sinensis,* for example. Similarly, Zn was found at significantly higher levels in Salicaceae and Betulaceae species, except for *O. carpinifolia* (Fig. 6). *O. carpinifolia, Z. serrata,* and *S. aquatica grandis* had on average 4 -5 times higher Fe content than *Q. acutissima* and *R. copallina* (Fig. 6C). The remaining 11 species had intermediate values. Mg was the element for which the largest variations in leaf content among tree species were observed. *A. ginnala*

and *R. copallina* had Mg leaf contents 4 to 5 times lower than those of *B. pendula*, *B papyrifera, U. pumila, S. alba* and *M. pomifera.* Leaf contents and associated statistical data for the entire ICP set of 16 elements are provided in supplemental Table S1.

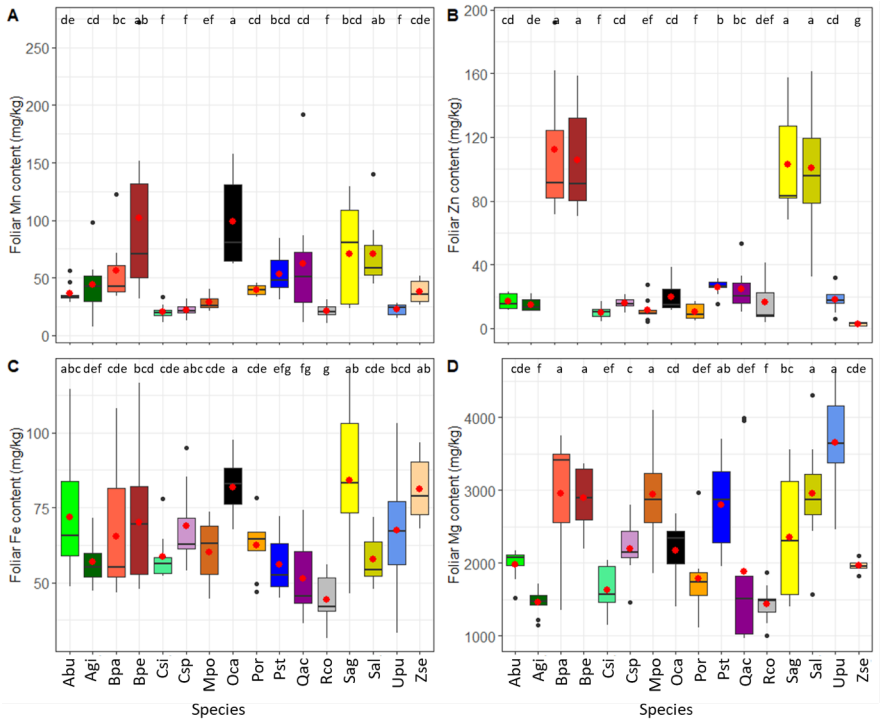

Fig. 6. Elemental content (mg/kg DM) (mean (red dot), median, quartiles, range, and outliers) (n=9) measured in leaves of the 16 tree species at the experimental Ochsenfeld site with (A) Mn, (B) Zn, (C) Fe and (D) Mg. Boxes with the same letter did not differ significantly from each other using a pairwise Kruskal−Wallis test ($P < 0.05$).

To highlight the potential concomitance between the foliar elemental content and transpiration stream proxies (g_{smax} and Ψ_{min}), the rank of the different tree species was obtained using the Spearman rank coefficient (Table 2). The species were ranked for g_{smax} significantly similarly to their foliar elemental contents in K, Mn (Fig. 6) and Sr. The relationship between leaf Mn content and g_{smax} showed that tree species that had a high Mn content also had high g_{smax} (*O. carpinifola*, *B. pendula*, and *S. alba*). Four of the tree species with the lowest g_{smax} also had low Mn contents (*A. ginnala*, *U. pumila*, *A. buergerianum*, and *C. sinensis*). *R. copallina* and *M. pomifera* combined a low foliar Mn content with high g_{smax} values.

Similarly, the Ψ_{min} values were also positively correlated with several elements, namely, Ca, Cd, Mg and Sr, and negatively correlated with Cu, Fe and Si. The other elements, *i.e.*, Al, B, Na, P, S, Ti and Zn, were only related to the tree species and did not correlate to any of the two transpiration proxies.

Table 2. Spearman rank-order correlation between g_{smax}, Ψ_{min}, and the foliar elemental content

*** P < 0.001, ** P < 0.01, * P < 0.05, ns = not significant

	Al	B	Ca	Cu	Cd	Fe	K	Mg	Mn	Na	P	S	Si	Sr	Ti	Zn
g_{smax}	ns	ns	ns	ns	ns	ns	*	ns	*	ns	ns	ns	ns	*	ns	ns
Ψ_{min}	ns	ns	**	*	**	*	ns	**	ns	ns	ns	ns	***	**	ns	ns

We further performed a 10-fold cross-validation confusion matrix on all tree species that includes all studied parameters (supplemental Table S2). A 80% generalized accuracy was determined, with 6 species showing 100% accuracy (Csi, Qac, Rco, Sal, Upu and Zse). Most of confusion occurred between species of the same plant genera (*e.g.* Bpa *versus* Bpe, Sal *versus* Sag*),* that showed similar g_{cmax} values (Fig. 5) and elemental content (Fig. 6). The g_{cmax} values contributed in increasing confusion among species of different genera (*e.g.* Qac *versus* Pst).

3.2. Growth chamber experiments

Five of the 16 tree species at the Ochsenfeld site were further chosen to analyse the transpiration rate and compare with field proxy data (measured after 90 and 152 days of growth). This will allow us to obtain quantitative transpiration rate data at the scale of the whole plant for each of the species studied, which is not easy to obtain at the field scale. *O. carpinifolia* had the highest transpiration rate, with a value greater than 1.5 mmol H_2O/leaf m^2/, which was higher than that for the other 4 tree species at day 90 (Fig. 7A). The transpiration rates were not significantly different at the intermediate time (90 days) and at the end time (152 days), except for *O. carpinifolia,* for which a significant decrease was observed, but its transpiration rate remained twice that of all other species. The rank order of these five tree species according to their transpiration rate was the same as that obtained with g_{smax} in the field experiment (*O. carpinifolia* > *B. pendula* > *S. aquatica grandis* > *P. stenoptera* > *A. buergerianum*).

The foliar Mn content of *B. pendula* was significantly higher (approximately 1000 mg/kg DM) than the Mn content of the other tree species, which values ranging from 100 to 400 mg/kg DM. *O. carpinifolia*

had an intermediate Mn content, which was significantly higher than that of *A. buergerianum*, *P. stenoptera* and *S. aquatica grandis* (Fig. 7B). There was no significant difference between the two measurement times despite a slight increase (1.2 on average) in leaf Mn content for *B. pendula,* which is a Mn-accumulating species. No significant rank-order correlation was observed between foliar Mn content and transpiration rate.

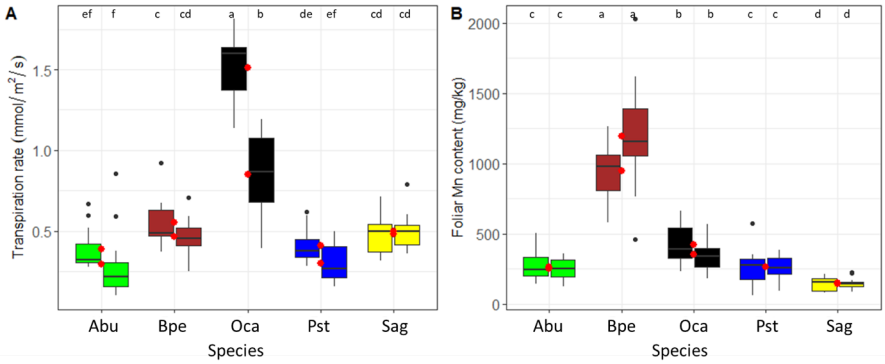

Fig. 7. (A) Transpiration rate (mmol H_2O/leaf m^2/s) and (B) leaf Mn content (mg/kg DM) (mean (red dot), median, quartiles, range, and outliers) (n = 24) measured on the 5 tree species grown in Ochsenfeld soil in chamber experiments. For each species, the first boxplot was measured at 90 days, and the second was measured at 152 days. Boxes with the same letter did not differ significantly from each other based on a pairwise Kruskal−Wallis test ($P < 0.05$).

4. Discussion

4.1. *O. carpinifolia* exhibited the highest transpiration capacity at the leaf level

According to their ecophysiological traits, the field experiment allowed us to identify three groups of tree species. The first group comprised *R. copallina* and *M. pomifera*, which had the highest g_{smax}, combined with the highest Ψ_{min} values, close to 0 MPa. We hypothesized that this performance of these two species could be due to their highly developed root system (Ciadamidaro, unpublished data), which provides them access to deep water, allowing them to maintain their Ψ_{min} close to zero despite a high maximum stomatal conductance to water vapour. The second group included *A. buergerianum* and *C. sinensis,* with the lowest g_{smax} and Ψ_{min}; the negative relationship among g_{smax} and CO_2 intercellular concentration underlines a biochemical limitation of the stomatal aperture, which is in agreement with their low growth performance. This group of tree species would not be able to grow optimally on this

site and could not be retained for revegetation. The third group was composed of all other tree species, including *O. carpinifolia*, characterized by a stomatal limitation of Ci concentration and a classical negative correlation between the stomatal aperture and leaf water potential (Comstock and Mencuccini, 1998; Cowan, 1965). Stomata regulate water loss from the leaves to maintain xylem pressure in a range that will protect xylem from embolism. Ψ_{50} is the xylem water potential provoking a 50% loss of hydraulic conductivity. At this potential, which is species-dependent, water transport in the xylem is highly impaired and can lead to drastic damage in the plant. In the current study, considering the Ψ_{min} between -2.27 and -0.09 MPa compared with Ψ_{50} recorded in the literature for the main temperate forest tree species (Choat et al., 2012), the water constraint was not sufficiently severe for all tree species to cause water transport damage. For example, we recorded a Ψ_{min} of -1.39 ± 0.1 MPa for *B. pendula* compared with a Ψ_{50} of -2.4 MPa that is known for this species (Herbette and Cochard, 2010). Ψ_{min} for *O. carpinifolia* was -1.81 ± 0.14 MPa in this study compared with a Ψ_{50} equal of -4.31 MPa in the study conducted by Kiorapostolou et al. (2019). In contrast, the Ψ_{min} of *S. aquatic grandis* was -1.22 ± 0.2 MPa and was close to the Ψ_{50} commonly described for this genus (-0.91 to -2.32 MPa) (Cochard et al., 1992), while no data are available in the literature for this species to date to the knowledge of the authors. Therefore, with a Ψ_{min} greater than Ψ_{50}, there was no risk for creating trapped gas emboli in the water transport system (Choat et al., 2012), and stomata should be fully or partially opened. Indeed, *Salix* species are well known to exhibit a high transpiration rate and would be interesting candidates to improve the evapotranspiration of landfills in phytomanagement solutions (Frédette et al., 2019). However, based on our site conditions, the stomatal limitation clearly moderated its performance, and the maximum stomatal conductance recorded for *B. pendula* or *O. carpinifolia* remained higher. Regarding the g_{smax} for *O. carpinifolia*, Tomasella et al. (2019) obtained values more than twice as high as ours, but *O. carpinifolia* was grown in a greenhouse under controlled conditions in pots containing lightweight substrate and potting compost irrigated at field capacity. Indeed, a measurement of g_{smax} over a few days would have been influenced by meteorological conditions, while we chose a sunny week and recorded a moderate decrease in Ψ_{min}. In our pot study under controlled conditions, a ranking similar to that obtained with the field experiment was found for the transpiration rate in well-irrigated conditions after three and five months of growth (Fig. 7), based on their g_{smax} values on a subset of species with different performances (*O. carpinifolia* > *B. pendula* > *S. aquatica grandis* > *P. stenoptera*

427 > *A. buergerianum*). Indeed, we should consider that g_{smax} measured during a few days of summer is a
428 good proxy of transpiration performance at the leaf level under these field conditions.

429 **4.2. *Ostrya carpinifolia* had the best growth performance, as estimated by UAV-based remote**
430 **sensing**

431 Among the 16 tree species that were planted in April 2014 at the Ochsenfeld site, *U. pumila*, *O.*
432 *carpinifolia*, *M. pomifera* and *S. aquatica* showed the highest growth (estimated by height) compared
433 with the other tree species, such as *B. pendula* or *Q. acutissima*. The species that had the greatest height
434 in our soil condition, *U. pumila,* was one of the dominant tree species at the Pingshuo mining landfill
435 located in northern Shanxi Province in China (Yuan et al., 2020); *U. pumila* is resistant to drought and
436 fast growing. *U. pumila* is a species with high adaptability to different climates: glacial temperate,
437 temperate and subtropical zones (Zhao et al., 2015). The *O. carpinifolia* species was one of the
438 intermediate-growing species in 2015 (direct height measurements, Ciadamidaro et al., 2019) but
439 became the best-performing tree species during our last measurement in 2018, after 4 years of growth
440 at the Ochsenfeld site. It also performed very well at two other phytomanagement sites (Ciadamidaro,
441 unpublished data). *O. carpinifolia* needs a low amount of resources for growth (Tardella et al., 2019)
442 and plays an important function in the forest vegetation in sub-Mediterranean areas in Italy at altitudes
443 lower than 1200 m. It has been described as a species capable of growing on shallow and poorly
444 developed soils, mainly on limestone and gypsum (Pasta et al., 2016). *M. pomifera* intrinsically has a
445 strong adaptive capacity in nutrient-poor soils and a high resistance to severe drought (Khaleghi et al.,
446 2019). The species belonging to the *Salix* genus is known to be a pioneer species suitable for cultivation
447 in difficult sites with suboptimal soil conditions (Kuzovkina and Volk, 2009). The authors of this review
448 explain that *Salix* species have a good adaptation to soil conditions, rapid growth, and the highest
449 biomass production obtained in short rotations, combined with high transpiration rates; therefore, *Salix*
450 species would be good candidates for phytomanagement in landfills. In contrast, *B. pendula,* which
451 spontaneously colonized the red gypsum landfill, (Zapata-Carbonell et al., 2019) did not grow well in
452 the experimental plot, probably because of the presence of other competing herbaceous species. *Betula*
453 species are known to be affected by planting density, which significantly reduces their crown and branch
454 sizes (Mäkinen, 2002; Wang et al., 2017). The poor growth of *Quercus* species observed at the

Ochsenfeld site could be explained by the intrinsic low-growth character of this genus and/or the vulnerability of the species to poor soil nutrient status and moisture deficiency (Demchik and Sharpe, 2000).

4.3. UAV-based surface integration method was innovatively applied to a landfill phytomanagement to estimate tree LAI and canopy conductance

The LAI values obtained in the present study by using the UAV-based surface integration method were within the same order as those found in previous studies. For instance, the LAI for *S. alba* and *S. aquatica grandis* were in the range of 2.1-3.4 leaf m²/ground m² in our study, comparable to the 1-5.5 leaf m²/ground m² range found for other *Salix* species (Mirck and Volk, 2009). In that study, the LAI values measured with a LI-COR LAI 2000 for *Salix*, one of the best shrub willow varieties growing at an industrial landfill, peaked during the beginning of July and August and were minimal in November. The LAI development course of poplar and willow clones was obtained, and LAI values also greatly varied during the season (Rüth et al., 2007). LAI values obtained during May in that study (which correspond to our sampling date) were in the 2-3 leaf m^2/ground m^2 range, similar to the values obtained for our *Salix* clones. *U. pumila* and *O. carpinifolia* had the highest LAI values in our study, which were also well correlated with tree heights. Similar relationships between vegetation height and LAI have been found in other studies (Luo et al., 2015; Rüth et al., 2007). The LAI values that varied on average from 0.23 to 0.40 leaf m²/ground m² for the different tree species studied at the Ochsenfeld site showed that the vegetation was dense because the NDVI of a densely vegetated plot or area tends towards positive values (Viana et al., 2019). Therefore, high NDVI values would indicate high NIR reflectance and low red reflectance related to high leaf density and/or high chlorophyll content, while low NDVI values would indicate a diminution of NIR reflectance indicating leaf damage or high red reflectance due to low leaf density. Indeed, the NDVI is intrinsically correlated to LAI by using the calculation mode but integrates chlorophyll content and leaf health (Tucker, 1979). In our study, except for *P. stenoptera,* the five tree species that had significantly higher NDVI values were the species with the greatest g_{smax} (*O. carpinifolia*, *R. copallina* and *M. pomifera*) and the highest LAI (*O. carpinifolia*, *U. pumila* and *S. aquatica grandis*). Despite a relatively low height, *P. stenoptera* had a high density of long and pinnately leaves, thus could have led to an underestimation of LAI with our method. Regardless, the low g_{cmax}

483 recorded for this species could be mainly attributed to its relatively low stomatal conductance compared
484 to other species with similar NDVI values. The species with the highest NDVI values, *i.e.*, *O.*
485 *carpinifolia*, also had the highest LAI value. These values reflect the acclimation of this tree species to
486 site conditions, as discussed above. Correlation coefficients of 0.77 and 0.99 between NDVI and LAI
487 were obtained at two sites for vegetation grown in a semiarid grassland (Fan et al., 2009). At these sites,
488 NDVI and LAI both reached peak values in August and became the maximum values. The present study
489 underlined that our LAI calculation was robust, as it correlated with the NDVI, the widely used spectral
490 reflectance index. The NDVI remains a qualitative proxy, *i.e.*, an index that needs to be calibrated with
491 LAI field measurements (Fan et al., 2009). The g_{cmax} proxy used in the present study was innovatively
492 measured by combining the surface integration method using UAV-based remote sensing and 3-D
493 imaging with traditional g_{smax} measurements and provided direct quantitative values allowing a better
494 comparison of different tree species performances. The negative point of this surface integration method
495 was the manual delineation of leaf area, which was tedious. With the rapid development of UAV
496 technology, UAV-based remote sensing has been widely used in forestry, agriculture, and vegetation
497 monitoring (Lu et al., 2020). UAV-based remote sensing has many advantages, such as instant
498 information acquisition, high image spatial resolution, convenient operation, high manoeuvrability,
499 freedom from cloud interference, and low cost. Our present study was in line with this, as it combined
500 remote sensing and gas exchange measurements to determine the canopy conductance of different tree
501 species. In view of the diversity of tree species used, other multispectral indices would have been
502 interesting to consider. These indices could take into account spectral ranges between 0.4-2.5 µm (Yang
503 et al., 2017). Remote sensing approaches based on thermal signature as a proxy of transpiration streams
504 (Xue and Su, 2017) through indices such as the Crop Water Stress Index (CWSI) could be used.
505 Evapotranspiration estimation at the field level requires water balance measurements using lysimetric
506 methods to collect sap flow measurements, as detailed in a review on classical methods (Rana and
507 Katerji, 2000), or modelling methods based on stomatal conductance measurements, meteorological
508 parameters and extractable soil water measurements (Granier et al., 2000). All of these methods are
509 quantitatively precise and have been improved well but are time-consuming and cannot be applied for
510 rapid screening of plant performance in phytomanagement contexts. However, a key parameter was the
511 estimation of a LAI that conditioned the evaporative surface. This LAI obtained by using the surface

integration method combined with g_{smax} allows us to obtain an estimation of the maximal canopy conductance g_{cmax}. Although this proxy is quantitative, it could not replace the methods cited above; however, it allowed obtaining a rapid comparison indicator of the difference in performance for the species to evaporate water at the landfill. We found that the best performing species should be *O. carpinifolia, M. pomifera, R. copallina, S. aquatic grandis, U. pumila* and *P. orientalis*. However, *R. copallina* behaved as an invasive species in the experimental plot at the Ochsenfeld site, which casts doubt on its potential use in phytomanagement scenarios. Although they performed very well in terms of growth, *S. aquatica grandis* and *U. pumila* with a Ψ_{min} close to Ψ_{50} and limited g_{smax} would be sensitive tree species in the event of drought. Therefore, we recommended only three species, *i.e.*, *O. carpinifolia, M. pomifera* and *P. orientalis*, to be utilized for phytomanagement at the Ochsenfeld site.

4.4. Mn uptake and transpiration rate were correlated

In our study, the concentrations of the different elements, including TEs (Table S1), were lower than those generally observed at anthropized sites (Kabata-Pendias, 2011). This might be because tree sampling was conducted in early summer, when the elemental concentrations were not yet at their optimal levels (Migeon et al., 2009). These authors demonstrated that the elemental content in the leaves collected in October was significantly higher than that collected in June, suggesting seasonal variability in the leaf elemental content. The other elemental contents found in our study were lower than the basal physiological compositions recorded in tree species (Fe=150 mg/kg DM, Mn=200 mg/kg DM and Zn=50 mg/kg DM) (Assad et al., 2017; Greger, 2004). Excess of these elements in plant tissues may cause toxicity by damaging the cell structure (Zhao et al., 2012) and therefore may affect plant growth and limit transpiration. With elemental contents slightly lower than usual physiological values, our tree species are therefore unlikely to have problems in their physiological processes, such as transpiration. However, Zn concentrations measured in *Betula* and *Salix* genera in the present field experiments were slightly higher than the physiological levels (Kabata-Pendias, 2011), which is consistent with our previous studies (Ciadamidaro et al., 2019; Zapata-Carbonell et al., 2020). Mn was also found to accumulate in *Betula* species in the present field experiment, which also confirms our previous data (Ciadamidaro et al., 2019; Zapata-Carbonell et al., 2020). In the pot experiment, high Mn content measured in the tree species in particular in *B. pendula*, could be explained by the conditions of the

experiment conducted in growth chamber, favorable for the accumulation of ET. However, the use of only five tree species in the laboratory experiment failed to show a rank-order correlation between Mn content and transpiration rate.

In addition to other factors, such as mobility of the element, tissue age, and biomass of the tree, water flow in the tree plays an important role in element uptake and translocation to the shoot, and water is necessary for circulation in the transpiration stream (Brown and Shelp, 1997). The foliar Mn content in some tree species grown in the red gypsum sediment at the Ochsenfeld site was correlated with the transpiration rate of the tree. Although the objective at the Ochsenfeld site is not to decontaminate the sediment, the choice of Mn-accumulating tree species with a high transpiration rate may be relevant to phytomining (Ent et al., 2018) or ecocatalysis processes (Escande et al., 2015). Xu et al. (2006) nicely reported that the Mn content in a leaf decreased by approximately 90% when it was wrapped in a transparent plastic bag to suppress the transpiration rate. In contrast, other elemental contents were not related to transpiration, *e.g.*, Zn uptake was not affected by the transpiration capacity of the tree species. Managing both metal uptake and water flow at landfills is therefore highly dependent on tree species and the elements of concern.

5. Conclusions

Here, we combined a UAV-based remote sensing approach and a surface integration method using 3D imagery to determine the LAI values of different species of trees planted in rows. This approach is an alternative to the long and tedious methods of dendrometric and ecophysiological measurements. We utilized the g_{cmax} (g_{smax} x LAI) proxy, which was found to be a relevant tool for evaluating the performance of selected trees at the Ochsenfeld site, and in particular for estimating the capacities of trees to manage water flows, compared with traditional proxies, such as NDVI, LAI or g_{smax} when considered separately. With the highest growth and g_{cmax} values compared with other planted woody species, *O. carpinifolia* had the greatest potential to maximize transpiration flows in these harsh conditions. These field measurements were confirmed by measurements performed under controlled conditions on the same substrate. *O. carpinifolia* also retained Mn in its leaves, similar to the other tree species in the Betulaceae family, *B. pendula*, even though Mn concentrations were highest under controlled conditions. This opens new perspectives in phytomining and ecocatalysis research domains

568 that combine phytomanagement with added values in the enriched biomass. High transpiration of the
569 woody cover obtained with this woody species could drastically reduce the volumes of water infiltrating
570 through the landfill and therefore limit the associated environmental risks and treatment costs. Species
571 more classically used in phytomanagement, such as those belonging to the Salicaceae (genus *Salix*), are
572 undoubtedly less relevant at this site because they have a much more limited potential transpiration rate.
573 In the event of multiple choices of tree species to manage these landfills, *M. pomifera* and *P. orientalis*
574 would be preferred tree species, in addition to *O. carpinifolia*. Their potential would now need to be
575 confirmed by, *e.g.,* a lysimeter installation for the accurate and representative measurements of the
576 evapotranspiration rate and water balance at the site. In the future, an atmospheric correction will be
577 provided to manipulate spectral reflectance at ground level to remove potential atmospheric effects. As
578 advanced sensors with large spectral diversity are being developed, we foresee the use of remote sensing
579 as a method to evaluate both plant and soil metal concentrations, and thus correlate metal concentration
580 and UAV-based ecophysiological parameters for a better assessment of phytomanagement strategies in
581 landfill restoration. Regarding the Ochsenfeld study site, which is representative of landfills from the
582 extractive industry, the key issue is the implementation of a plant cover that maximizes water
583 evapotranspiration after deposits have ceased and that limits the aerial dissemination of red gypsum
584 dust, which is imposed by the French regulator. The presence of trees with high evapotranspiration
585 capacities would allow to maximize these impacts. Additionally, we are foreseeing the use of
586 phytomining in future projects to recover metals from the plant biomasses. However, given the huge
587 amounts of metals in the substrate, it would be inappropriate to expect metal depollution.
588

589 **CRediT authorship contribution statement**

590 Abdoulaye Mahamat Malabad: Investigation, Writing -original draft; Fabienne Tatin-Froux and Julien
591 Parelle: Investigation, Writing -original draft; Gilles Gallinet: UAV acquisition, Writing -original draft;
592 Jean-Michel Colin: Writing -original draft, site maintenance; and Michel Chalot: Writing - review &
593 editing, Funding acquisition, Supervision.

Declaration of Competing Interest

The authors declare that they have no known competing financial interests or personal relationships that could have appeared to influence the work reported in this paper.

Acknowledgement

We acknowledge Dr. Nadia Morin-Crini, Marie-Laure Toussaint and Caroline Amiot of the PEAT² platform for the metal analyses. This work was supported by the French National Research Agency [PHYTOCHEM ANR-13-CDII-0005-01] and the French Environment and Energy Management Agency [PROLIPHYT ADEME- 1172C0053]. A.M.M. received a PhD grant from the Ministry of Higher Education, Research and Innovation of the Republic of Chad [561 PR/MESRI/SG/DGCNOU/DEPOB/SEPOB/2018].

References

Adhikari, T., Rattan, R.K., 2000. Modelling zinc uptake by rice crop using a Barber-Cushman approach. Plant and Soil 227, 235–242. https://doi.org/10.1023/A:1026575032724

Aggarwal, A., Sharma, I., Tripathi, B., Munjal, A., Baunthiyal, M., Sharma, V., 2011. Metal Toxicity and Photosynthesis, in: Photosynthesis: Overviews on Recent Progress and Future Perspectives. pp. 16: 229-236.

Alonzo, M., Bookhagen, B., McFadden, J.P., Sun, A., Roberts, D.A., 2015. Mapping urban forest leaf area index with airborne lidar using penetration metrics and allometry. Remote Sensing of Environment 162, 141–153. https://doi.org/10.1016/j.rse.2015.02.025

Arsenov, D., Nikolić, N., Borišev, M., Župunski, M., Pilipovic, A., Orlović, S., Pajević, S., 2020. Greenhouse Assessment of Citric Acid-Assisted Phytoremediation of Cadmium by Willows (Salix spp.) □ Effect on Photosynthetic Performances and Metal Tolerance. Baltic Forestry 25, 203–212. https://doi.org/10.46490/vol25iss2pp203

Assad, M., Tatin-Froux, F., Blaudez, D., Chalot, M., Parelle, J., 2017. Accumulation of trace elements in edible crops and poplar grown on a titanium ore landfill. Environ Sci Pollut Res 24, 5019–5031. https://doi.org/10.1007/s11356-016-8242-4

Barber, S.A., 1995. Soil Nutrient Bioavailability: A Mechanistic Approach. John Wiley & Sons.

Breda, N.J.J., 2003. Ground-based measurements of leaf area index: a review of methods, instruments and current controversies. Journal of Experimental Botany 54, 2403–2417. https://doi.org/10.1093/jxb/erg263

Brouder, S.M., 1994. Evaluation of a Mechanistic Model of Potassium Uptake by Cotton in Vermiculitic Soil. Soil Science Society of America journal v. 58, 1174–1183. https://doi.org/10.2136/sssaj1994.03615995005800040024x

Brown, P.H., Shelp, B.J., 1997. Boron mobility in plants. Plant and Soil 193, 85–101. https://doi.org/10.1023/A:1004211925160

Chandra, R., Kang, H., 2016. Mixed heavy metal stress on photosynthesis, transpiration rate, and chlorophyll content in poplar hybrids. Forest Science and Technology 12, 55–61. https://doi.org/10.1080/21580103.2015.1044024

Chen, J.-H., 1990. Soil pH and Phosphorus and Potassium Uptake by Maize Evaluated with an Uptake Model. Soil Science Society of America journal v. 54, 1032–1036. https://doi.org/10.2136/sssaj1990.03615995005400040017x

Choat, B., Jansen, S., Brodribb, T.J., Cochard, H., Delzon, S., Bhaskar, R., Bucci, S.J., Feild, T.S., Gleason, S.M., Hacke, U.G., Jacobsen, A.L., Lens, F., Maherali, H., Martínez-Vilalta, J., Mayr, S., Mencuccini, M., Mitchell, P.J., Nardini, A., Pittermann, J., Pratt, R.B., Sperry, J.S., Westoby, M., Wright, I.J., Zanne, A.E., 2012. Global convergence in the vulnerability of forests to drought. Nature 491, 752–755. https://doi.org/10.1038/nature11688

Ciadamidaro, L., Parelle, J., Tatin-Froux, F., Moyen, C., Durand, A., Zappelini, C., Morin-Crini, N., Soupe, D., Blaudez, D., Chalot, M., 2019. Early screening of new accumulating versus non-accumulating tree species for the phytomanagement of marginal lands. Ecological Engineering 130, 147–156. https://doi.org/10.1016/j.ecoleng.2019.02.010

Cochard, H., Cruiziat, P., Tyree, M.T., 1992. Use of Positive Pressures to Establish Vulnerability Curves: Further Support for the Air-Seeding Hypothesis and Implications for Pressure-Volume Analysis. Plant Physiol. 100, 205–209. https://doi.org/10.1104/pp.100.1.205

Comstock, J., Mencuccini, M., 1998. Control of stomatal conductance by leaf water potential in Hymenoclea salsola (T. & G.), a desert subshrub. Plant Cell Environ 21, 1029–1038. https://doi.org/10.1046/j.1365-3040.1998.00353.x

Cowan, I.R., 1965. Transport of Water in the Soil-Plant-Atmosphere System. The Journal of Applied Ecology 2, 221. https://doi.org/10.2307/2401706

Cundy, A.B., Bardos, R.P., Puschenreiter, M., Mench, M., Bert, V., Friesl-Hanl, W., Müller, I., Li, X.N., Weyens, N., Witters, N., Vangronsveld, J., 2016. Brownfields to green fields: Realising wider benefits from practical contaminant phytomanagement strategies. Journal of Environmental Management 184, 67–77. https://doi.org/10.1016/j.jenvman.2016.03.028

Demchik, M.C., Sharpe, W.E., 2000. The effect of soil nutrition, soil acidity and drought on northern red oak (Quercus rubra L.) growth and nutrition on Pennsylvania sites with high and low red

a mis en forme : Anglais (E.U.)

oak mortality. Forest Ecology and Management 136, 199–207. https://doi.org/10.1016/S0378-1127(99)00307-2

Drisya, J., D, S.K., Roshni, T., 2018. Chapter 27 - Spatiotemporal Variability of Soil Moisture and Drought Estimation Using a Distributed Hydrological Model, in: Samui, P., Kim, D., Ghosh, C. (Eds.), Integrating Disaster Science and Management. Elsevier, pp. 451–460. https://doi.org/10.1016/B978-0-12-812056-9.00027-0

Ducic, T., Polle, A., 2005. Transport and detoxification of manganese and copper in plants. Braz. J. Plant Physiol. 17, 103–112. https://doi.org/10.1590/S1677-04202005000100009

Edraki, M., Baumgartl, T., Manlapig, E., Bradshaw, D., Franks, D.M., Moran, C.J., 2014. Designing mine tailings for better environmental, social and economic outcomes: a review of alternative approaches. Journal of Cleaner Production 84, 411–420. https://doi.org/10.1016/j.jclepro.2014.04.079

Ent, A. van der, Echevarria, G., Baker, A.J.M., Morel, J.L. (Eds.), 2018. Agromining: Farming for Metals: Extracting Unconventional Resources Using Plants, Mineral Resource Reviews. Springer International Publishing. https://doi.org/10.1007/978-3-319-61899-9

Escande, V., Velati, A., Garel, C., Renard, B.-L., Petit, E., Grison, C., 2015. Phytoextracted mining wastes for ecocatalysis: Eco-Mn®, an efficient and eco-friendly plant-based catalyst for reductive amination of ketones. Green Chem. 17, 2188–2199. https://doi.org/10.1039/C4GC02193B

Fan, L., Gao, Y., Brück, H., Bernhofer, Ch., 2009. Investigating the relationship between NDVI and LAI in semi-arid grassland in Inner Mongolia using in-situ measurements. Theor Appl Climatol 95, 151–156. https://doi.org/10.1007/s00704-007-0369-2

Fernando, D.R., Marshall, A.T., Forster, P.I., Hoebee, S.E., Siegele, R., 2013. Multiple metal accumulation within a manganese-specific genus. American Journal of Botany 100, 690–700. https://doi.org/10.3732/ajb.1200545

Frédette, C., Labrecque, M., Comeau, Y., Brisson, J., 2019. Willows for environmental projects: A literature review of results on evapotranspiration rate and its driving factors across the genus Salix. Journal of Environmental Management 246, 526–537. https://doi.org/10.1016/j.jenvman.2019.06.010

Gandhi, G.M., Parthiban, S., Thummalu, N., Christy, A., 2015. Ndvi: Vegetation Change Detection Using Remote Sensing and Gis – A Case Study of Vellore District. Procedia Computer Science 57, 1199–1210. https://doi.org/10.1016/j.procs.2015.07.415

Gessesse, A.A., Melesse, A.M., 2019. Temporal relationships between time series CHIRPS-rainfall estimation and eMODIS-NDVI satellite images in Amhara Region, Ethiopia, in: Extreme Hydrology and Climate Variability. Elsevier, pp. 81–92. https://doi.org/10.1016/B978-0-12-815998-9.00008-7

Granier, A., Loustau, D., Bréda, N., 2000. A generic model of forest canopy conductance dependent on climate, soil water availability and leaf area index. Ann. For. Sci. 57, 755–765. https://doi.org/10.1051/forest:2000158

Greger, M., 2004. Metal Availability, Uptake, Transport and Accumulation in Plants, in: Prasad, M.N.V. (Ed.), Heavy Metal Stress in Plants. Springer Berlin Heidelberg, Berlin, Heidelberg, pp. 1–27. https://doi.org/10.1007/978-3-662-07743-6_1

Herbette, S., Cochard, H., 2010. Calcium Is a Major Determinant of Xylem Vulnerability to Cavitation. Plant Physiol. 153, 1932–1939. https://doi.org/10.1104/pp.110.155200

Huang, G., Hayes, P.E., Ryan, M.H., Pang, J., Lambers, H., 2017. Peppermint trees shift their phosphorus-acquisition strategy along a strong gradient of plant-available phosphorus by increasing their transpiration at very low phosphorus availability. Oecologia 185, 387–400. https://doi.org/10.1007/s00442-017-3961-x

Huang, L., Baumgartl, T., Mulligan, D., 2012. Is rhizosphere remediation sufficient for sustainable revegetation of mine tailings? Annals of Botany 110, 223–238. https://doi.org/10.1093/aob/mcs115

Hunt, E.R., Hively, W.D., Daughtry, C.S.T., McCarty, G.W., Fujikawa, S.J., Ng, T.L., Tranchitella, M., Linden, D.S., Yoel, D.W., Microsystems, I., Drive, T., 2008. REMOTE SENSING OF CROP LEAF AREA INDEX USING UNMANNED AIRBORNE VEHICLES 9. In ASPRS Pecora 17 Conference Proceeding, Bethesda, MD: American Society for Photogrammetry and Remote Sensing. http://www.asprs.org/a/publications/proceedings/pecora17/0018.pdf.

Joint Research Centre, 2017. Large-scale physical and chemical land disturbance. [WWW Document]. WAD | World Atlas of Desertification. URL https://wad.jrc.ec.europa.eu/mining (accessed 3.22.21).
Kabata-Pendias, A., 2011. Trace elements in soils and plants, 4th ed. ed. CRC Press, Boca Raton.
Kasim, W.A., 2007. Physiological Consequences of Structural and Ultra-structural Changes Induced by Zn Stress in Phaseolus vulgaris. II. Enzymes, Amino Acids and Protein Profile. International Journal of Botany. https://doi.org/10.3923/ijb.2007.33.39
Khaleghi, A., Naderi, R., Brunetti, C., Maserti, B.E., Salami, S.A., Babalar, M., 2019. Morphological, physiochemical and antioxidant responses of Maclura pomifera to drought stress. Sci Rep 9, 19250. https://doi.org/10.1038/s41598-019-55889-y
Kiorapostolou, N., Da Sois, L., Petruzzellis, F., Savi, T., Trifilò, P., Nardini, A., Petit, G., 2019. Vulnerability to xylem embolism correlates to wood parenchyma fraction in angiosperms but not in gymnosperms. Tree Physiology 39, 1675–1684. https://doi.org/10.1093/treephys/tpz068
Kitao, M., Lei, T.T., Koike, T., 1997. Comparison of photosynthetic responses to manganese toxicity of deciduous broad-leaved trees in northern Japan. Environmental Pollution 97, 113–118. https://doi.org/10.1016/S0269-7491(97)00064-X
Kuzovkina, Y.A., Volk, T.A., 2009. The characterization of willow (Salix L.) varieties for use in ecological engineering applications: Co-ordination of structure, function and autecology. Ecological Engineering 35, 1178–1189. https://doi.org/10.1016/j.ecoleng.2009.03.010
Lefsky, M.A., Cohen, W.B., Acker, S.A., Parker, G.G., Spies, T.A., Harding, D., 1999. Lidar Remote Sensing of the Canopy Structure and Biophysical Properties of Douglas-Fir Western Hemlock Forests. Remote Sensing of Environment 70, 339–361.
Levene, H., 1960. Essays in Honor of Harold Hotelling, in: In Contributions to Probability and Statistics. Stanford University Press, Palo Alto, CA., pp. 278–292.
Lin, L., Yu, K., Yao, X., Deng, Y., Hao, Z., Chen, Y., Wu, N., Liu, J., 2021. UAV Based Estimation of Forest Leaf Area Index (LAI) through Oblique Photogrammetry. Remote Sensing 13, 803. https://doi.org/10.3390/rs13040803
Lin, Y., 2015. LiDAR: An important tool for next-generation phenotyping technology of high potential for plant phenomics? Computers and Electronics in Agriculture 119, 61–73. https://doi.org/10.1016/j.compag.2015.10.011
Loudermilk, E.L., Hiers, J.K., O'Brien, J.J., Mitchell, R.J., Singhania, A., Fernandez, J.C., Cropper, W.P., Slatton, K.C., 2009. Ground-based LIDAR: a novel approach to quantify fine-scale fuelbed characteristics. Int. J. Wildland Fire 18, 676. https://doi.org/10.1071/WF07138
Lu, H., Fan, T., Ghimire, P., Deng, L., 2020. Experimental Evaluation and Consistency Comparison of UAV Multispectral Minisensors. Remote Sensing 12, 2542. https://doi.org/10.3390/rs12162542
Luo, S., Wang, C., Pan, F., Xi, X., Li, G., Nie, S., Xia, S., 2015. Estimation of wetland vegetation height and leaf area index using airborne laser scanning data. Ecological Indicators 48, 550–559. https://doi.org/10.1016/j.ecolind.2014.09.024
Mäkinen, H., 2002. Effect of stand density on the branch development of silver birch (Betula pendula Roth) in central Finland. Trees 16, 346–353. https://doi.org/10.1007/s00468-002-0162-x
Migeon, A., Richaud, P., Guinet, F., Chalot, M., Blaudez, D., 2009. Metal Accumulation by Woody Species on Contaminated Sites in the North of France. Water Air Soil Pollut 204, 89–101. https://doi.org/10.1007/s11270-009-0029-5
Milan, B., 2012. Response of Salix alba L. to heavy metals and diesel fuel contamination. African Journal of Biotechnology 11. https://doi.org/10.5897/AJB12.1004
Mirck, J., Volk, T.A., 2009. Seasonal Sap Flow of Four *Salix* Varieties Growing on the Solvay Wastebeds in Syracuse, NY, USA. International Journal of Phytoremediation 12, 1–23. https://doi.org/10.1080/15226510902767098
Nowak, D., 1996. Notes: Estimating Leaf Area and Leaf Biomass of Open-Grown Deciduous Urban Trees. Forest Science 42, 504–507.
Page, V., Weisskopf, L., Feller, U., 2006. Heavy metals in white lupin: uptake, root-to-shoot transfer and redistribution within the plant. New Phytol 171, 329–341. https://doi.org/10.1111/j.1469-8137.2006.01756.x
Pajevic, S., Borisev, M., Nikolic, N., Krstic, B., Pilipovic, A., Orlovic, S., 2009. Phytoremediation capacity of poplar (Populus spp.) and willow (Salix spp.) clonesin relation to photosynthesis. Archives of Biological Sciences 61, 239–247. https://doi.org/10.2298/ABS0902239P

a mis en forme : Français

772 Pandey, N., Sharma, C.P., 2003. Chromium interference in iron nutrition and water relations of cabbage.
773 Environmental and Experimental Botany 49, 195–200. https://doi.org/10.1016/S0098-
774 8472(02)00088-6
775 Pasta, S., de Rigo, D., Caudullo, G., 2016. Ostrya carpinifolia in Europe: distribution, habitat, usage and
776 threats 2.
777 Peper, P.J., McPherson, E.G., 1998. Comparison of five methods for estimating leaf area index of open-
778 grown deciduous trees 14.
779 QGIS Development Team, 2018. QGIS Geographic Information System: Open Source Geospatial
780 Foundation Project.
781 R Core Team, 2021. R: A language and environment for statistical computing. Vienna, Austria: R
782 Foundation for Statistical Computing.
783 Rana, G., Katerji, N., 2000. Measurement and estimation of actual evapotranspiration in the field under
784 Mediterranean climate: a review. European Journal of Agronomy 13, 125–153.
785 https://doi.org/10.1016/S1161-0301(00)00070-8
786 Rauhala, A., Tuomela, A., Davids, C., Rossi, P.M., 2017. UAV Remote Sensing Surveillance of a Mine
787 Tailings Impoundment in Sub-Arctic Conditions. Remote Sensing 9, 1318.
788 https://doi.org/10.3390/rs9121318
789 Robinson, B.H., Green, S.R., Chancerel, B., Mills, T.M., Clothier, B.E., 2007. Poplar for the
790 phytomanagement of boron contaminated sites. Environmental Pollution 150, 225–233.
791 https://doi.org/10.1016/j.envpol.2007.01.017
792 Rüth, B., Lennartz, B., Kahle, P., 2007. Water regime of mechanical—biological pretreated waste
793 materials under fast-growing trees. Waste Manag Res 25, 408–416.
794 https://doi.org/10.1177/0734242X07076940
795 Sadana, U.S., Claassen, N., 2000. Manganese dynamics in the rhizosphere and Mn uptake by different
796 crops evaluated by a mechanistic model. Plant and Soil 218, 233–238.
797 https://doi.org/10.1023/A:1014964107614
798 Scholander, P.F., Bradstreet, E.D., Hemmingsen, E.A., Hammel, H.T., 1965. Sap Pressure in Vascular
799 Plants: Negative hydrostatic pressure can be measured in plants. Science 148, 339–346.
800 https://doi.org/10.1126/science.148.3668.339
801 Shahmoradi, J., Talebi, E., Roghanchi, P., Hassanalian, M., 2020. A Comprehensive Review of
802 Applications of Drone Technology in the Mining Industry. Drones 4, 34.
803 https://doi.org/10.3390/drones4030034
804 Shapiro, S.S., Wilk, M.B., 1965. An Analysis of Variance Test for Normality (Complete Samples).
805 Biometrika 52, 591–611. https://doi.org/10.2307/2333709
806 Tardella, F.M., Postiglione, N., Tavoloni, M., Catorci, A., 2019. Changes in species and functional
807 composition in the herb layer of sub-Mediterranean Ostrya carpinifolia abandoned coppices.
808 Plant Ecol 220, 1043–1055. https://doi.org/10.1007/s11258-019-00973-6
809 Tavanti, R.F.R., David Queiroz, G., Caroline Da Rocha Silva, A., Moya Peres, W., Pereira Paixão, A.,
810 Galindo, F.S., Martins Silva, V., Bossolani, J.W., Moreira Melero, M., De Souza Oliveira, G.,
811 Furlani Júnior, E., Dos Reis, A.R., 2019. Changes in photosynthesis and antioxidant metabolism
812 of cotton (*Gossypium hirsutum* L.) plants in response to manganese stress. Archives of
813 Agronomy and Soil Science 1–20. https://doi.org/10.1080/03650340.2019.1637857
814 Tian, J., Wang, L., Li, X., Gong, H., Shi, C., Zhong, R., Liu, X., 2017. Comparison of UAV and
815 WorldView-2 imagery for mapping leaf area index of mangrove forest. International Journal of
816 Applied Earth Observation and Geoinformation 61, 22–31.
817 https://doi.org/10.1016/j.jag.2017.05.002
818 Tomasella, M., Casolo, V., Aichner, N., Petruzzellis, F., Savi, T., Trifilò, P., Nardini, A., 2019. Non-
819 structural carbohydrate and hydraulic dynamics during drought and recovery in Fraxinus ornus
820 and Ostrya carpinifolia saplings. Plant Physiology and Biochemistry 145, 1–9.
821 https://doi.org/10.1016/j.plaphy.2019.10.024
822 Tucker, C.J., 1979. Red and photographic infrared linear combinations for monitoring vegetation.
823 Remote Sensing of Environment 8, 127–150. https://doi.org/10.1016/0034-4257(79)90013-0
824 Van Assche, F., Ceulemans, R., Clijsters, H., 1980. Zinc mediated effects on leaf CO2 diffusion
825 conductances and net photosynthesis in Phaseolus vulgaris L. Photosynthesis Research 1, 171–
826 180. https://doi.org/10.1007/BF00020596
827 Vaverková, 2019. Landfill Impacts on the Environment— Review. Geosciences 9, 431.
828 https://doi.org/10.3390/geosciences9100431

Vernay, P., Gauthier-Moussard, C., Hitmi, A., 2007. Interaction of bioaccumulation of heavy metal chromium with water relation, mineral nutrition and photosynthesis in developed leaves of Lolium perenne L. Chemosphere 68, 1563–1575. https://doi.org/10.1016/j.chemosphere.2007.02.052

Viana, C.M., Oliveira, S., Oliveira, S.C., Rocha, J., 2019. Land Use/Land Cover Change Detection and Urban Sprawl Analysis, in: Spatial Modeling in GIS and R for Earth and Environmental Sciences. Elsevier, pp. 621–651. https://doi.org/10.1016/B978-0-12-815226-3.00029-6

Wang, C.-S., Zeng, Ji, Hein, S., Zhao, Z.-G., Guo, J.-J., Zeng, Jie, 2017. Crown and branch attributes of mid-aged *Betula alnoides* plantations in response to planting density. Scandinavian Journal of Forest Research 32, 679–687. https://doi.org/10.1080/02827581.2016.1261936

Wang, Y., Fang, H., 2020. Estimation of LAI with the LiDAR Technology: A Review. Remote Sensing 12, 3457. https://doi.org/10.3390/rs12203457

Watson, D.J., 1947. Comparative physiological studies on the growth of field crops. Ann Applied Biology 40, 1–37. https://doi.org/10.1111/j.1744-7348.1953.tb02364.x

Wilhelm, W.W., Ruwe, K., Schlemmer, M.R., 2000. Comparison of Three Leaf Area Index Meters in a Corn Canopy. Crop Science 40, 1179–1183. https://doi.org/10.2135/cropsci2000.4041179x

Xu, X., Shi, J., Chen, Y., Chen, X., Wang, H., Perera, A., 2006. Distribution and mobility of manganese in the hyperaccumulator plant Phytolacca acinosa Roxb. (Phytolaccaceae). Plant Soil 285, 323–331. https://doi.org/10.1007/s11104-006-9018-2

Xue, J., Su, B., 2017. Significant Remote Sensing Vegetation Indices: A Review of Developments and Applications. Journal of Sensors 2017, 1–17. https://doi.org/10.1155/2017/1353691

Yao, X., Wang, N., Liu, Y., Cheng, T., Tian, Y., Chen, Q., Zhu, Y., 2017. Estimation of Wheat LAI at Middle to High Levels Using Unmanned Aerial Vehicle Narrowband Multispectral Imagery. Remote Sensing 9, 1304. https://doi.org/10.3390/rs9121304

Yuan, Y., Ren, Y., Gao, G., Zhao, Z., Niu, S., 2020. Intra- and Interspecific Interactions among Pioneer Trees Affect Forest-Biomass Carbon Accumulation in a Nutrient-Deficient Reclaimed Coal Mine Spoil. Forests 11, 819. https://doi.org/10.3390/f11080819

Zapata-Carbonell, J., Bégeot, C., Carry, N., Choulet, F., Delhautal, P., Gillet, F., Girardclos, O., Mouly, A., Chalot, M., 2019. Spontaneous ecological recovery of vegetation in a red gypsum landfill: Betula pendula dominates after 10 years of inactivity. Ecological Engineering 132, 31–40. https://doi.org/10.1016/j.ecoleng.2019.03.013

Zapata-Carbonell, J., Ciadamidaro, L., Parelle, J., Chalot, M., Tatin-Froux, F., 2020. Improving Silver Birch (Betula pendula) Growth and Mn Accumulation in Residual Red Gypsum Using Organic Amendments. Front. Environ. Sci. 8, 24. https://doi.org/10.3389/fenvs.2020.00024

Zarco-Tejada, P.J., González-Dugo, V., Berni, J.A.J., 2012. Fluorescence, temperature and narrow-band indices acquired from a UAV platform for water stress detection using a micro-hyperspectral imager and a thermal camera. Remote Sensing of Environment 117, 322–337. https://doi.org/10.1016/j.rse.2011.10.007

Zhang, C., Kovacs, J.M., 2012. The application of small unmanned aerial systems for precision agriculture: a review. Precision Agric 13, 693–712. https://doi.org/10.1007/s11119-012-9274-5

Zhao, H., Wu, L., Chai, T., Zhang, Y., Tan, J., Ma, S., 2012. The effects of copper, manganese and zinc on plant growth and elemental accumulation in the manganese-hyperaccumulator Phytolacca americana. Journal of Plant Physiology 169, 1243–1252. https://doi.org/10.1016/j.jplph.2012.04.016

Zhao, Z., Wang, L., Bai, Z., Pan, Z., Wang, Y., 2015. Development of population structure and spatial distribution patterns of a restored forest during 17-year succession (1993–2010) in Pingshuo opencast mine spoil, China. Environ Monit Assess 187, 431. https://doi.org/10.1007/s10661-015-4391-z